

Intrinsic antiferromagnetic topological insulator and axion state in V_2WS_4

Yadong Jiang,^{1,2} Huan Wang,^{1,2} Kejie Bao,^{1,2} and Jing Wang^{1,2,3,4,*}

¹*State Key Laboratory of Surface Physics and Department of Physics, Fudan University, Shanghai 200433, China*

²*Shanghai Research Center for Quantum Sciences, Shanghai 201315, China*

³*Institute for Nanoelectronic Devices and Quantum Computing, Fudan University, Shanghai 200433, China*

⁴*Hefei National Laboratory, Hefei 230088, China*

(Dated: January 7, 2025)

Intrinsic magnetic topological insulators offer an ideal platform to explore exotic topological phenomena, such as axion electrodynamics, quantum anomalous Hall (QAH) effect and Majorana edge modes. However, these emerging new physical effects have rarely been experimentally observed due to the limited choice of suitable materials. Here, we predict the van der Waals layered V_2WS_4 and its related materials show intralayer ferromagnetic and interlayer antiferromagnetic exchange interactions. We find extremely rich magnetic topological states in V_2WS_4 , including an antiferromagnetic topological insulator, the axion state with the long-sought quantized topological magnetoelectric effect, three-dimensional QAH state, as well as a collection of QAH insulators and intrinsic axion insulators in odd- and even-layer films, respectively. Remarkably, the Néel temperature of V_2WS_4 is predicted to be much higher than that of $MnBi_2Te_4$. These interesting predictions, if realized experimentally, could greatly promote the topological quantum physics research and application.

The discovery of intrinsic magnetic topological insulators (TIs) [1–6] has opened new avenues for realizing a wide range of exotic topological phenomena through the time-reversal-breaking topological surface states [7–34]. A paradigm example is the realization of the quantum anomalous Hall (QAH) effect and axion insulator in few layer $MnBi_2Te_4$ [35–41]. Despite progress, experimental studies of magnetic topological states lag significantly behind their non-magnetic counterparts due to the limited availability of magnetic TI materials. While hundreds of intrinsic magnetic topological materials have been identified by symmetry-based analysis [42–47], *ab initio* calculations [48] and machine learning approaches [49], the vast majority are semimetals. To date, $MnBi_2Te_4$ remains the only experimentally confirmed intrinsic antiferromagnetic (AFM) TI [38, 39]. However, $MnBi_2Te_4$ has a relatively low Néel temperature, and its complex magnetic structure, coupled with imperfect sample quality, has hindered direct observation of the exchange gap in Dirac surface states using spectroscopy measurements [39, 50–52]. Thus, the search for realistic intrinsic magnetic TIs, preferably with higher magnetic ordering temperatures and large gaps, has become an important goal in topological material research. In this context, the class of V_2WS_4 materials predicted in this paper offer a promising solution. These materials feature high Néel temperatures and provide an ideal platform for exploring emergent magnetic topological phenomena, such as AFM TIs, the topological axion state with topological magnetoelectric effect (TME), and the QAH effect in both two- and three-dimensional (3D) systems, and so on.

Structure and magnetic properties.— The ternary transition metal chalcogenide V_2MX_4 , with $M = W$ or Mo , $X = S$ or Se , crystallize in an orthorhombic crystal structure with the space group $I\bar{4}2m$ (No. 121) with seven atoms in one primitive cell. Taking V_2WS_4 as

an example, it has a layered structure with a tetragonal lattice V_2WS_4 as the building block shown in Fig. 1. The key symmetry operation is $S_{4z} \equiv \mathcal{I}C_{4z}$, where \mathcal{I} is inversion symmetry. Each layer contains three atomic sub-layers (i.e. one V_2W and two S_2), where each V or W atom is surrounded by four S atoms forming a distorted edge-sharing tetrahedron. The layers of bulk V_2WS_4 are connected by van der Waals interactions and stack along z axis, forming an AB stacking pattern, which is energetically favorable than AA stacking [53]. The B layer can be regarded as A layer translating along $\tau_{1/2} = (a, a, c)/2$, where $(a, c) = (5.79, 9.55)$ Å are the in-plane and out-of plane lattice constant, respectively. The dynamical stability of V_2WS_4 is confirmed by first-principles phonon calculations [53]. Moreover, Cu_2MX_4 and Ag_2MX_4 with the same structure have been successfully synthesized [54–57], implying that these materials could potentially be fabricated experimentally.

First-principles density functional theory (DFT) calculations are employed to investigate the electronic structure of V_2WS_4 , with detailed methods provided in Supplemental Material [53]. Our analysis reveals that each V atom has a valence of +2 by losing its two $4s$ electrons. Total energy calculations for various magnetic structures of 3D V_2WS_4 were performed, as summarized in Fig. 1(e). The results show that the A-type AFM state with an out-of-plane easy axis (denoted as AFM- z) is the magnetic ground state. In this configuration, the material is ferromagnetic (FM) within the xy plane of each layer and AFM between adjacent layers along the z direction [Fig 1(d)]. The total energy of A-type AFM state with in-plane easy axis (AFM- x) is slightly higher than that of AFM- z , but significantly lower than FM- z state with an out-of-plane easy axis. This indicates that the magnetic anisotropy energy is weaker than the effective magnetic exchange interaction between neigh-

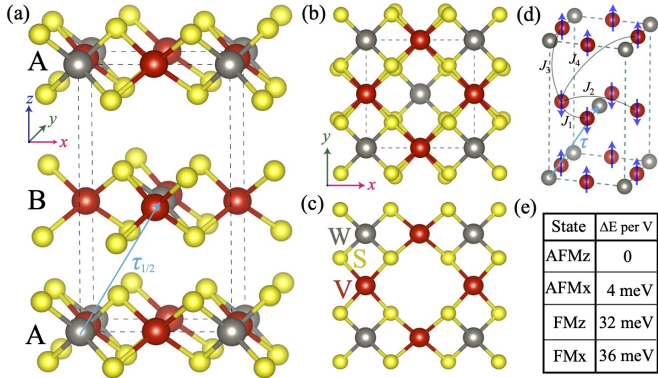


FIG. 1. Crystal and magnetic structures. (a) The unit cell of AFM V_2WS_4 consists of two layers with AB stacking. The cyan arrow denotes the half translation operator $\tau_{1/2}$. (b) The top view along the z axis. (c) The monolayer atomic structure from top view. (d) The magnetic AFM- z ground state. J_i denote the leading magnetic couplings between V-V pairs, and negative J_i means FM exchange coupling. $J_1 = -13.0$ meV, $J_2 = -7.5$ meV only represents intralayer next-nearest-neighbor V-V pairs through W atoms, $J_3 = 1.7$ meV and $J_4 = 1.4$ meV represent the two strongest interlayer couplings. (e) The calculated total energy for different magnetic ordered states.

boring layers. The calculated magnetic moments are primarily contributed by V ($\approx 2.6\mu_B$), with a smaller contribution from W ($\approx 0.4\mu_B$), confirming that the magnetism originates from the V atoms. This fractional magnetic moment arises from the band inversion between V $d_{xz,yz}$ orbitals and W d_{z^2} orbital [Fig. 2(a)]. The tetrahedral crystal field splits V $3d$ orbitals into lower-energy $e_g(d_{z^2}, d_{x^2-y^2})$ and higher-energy triplet $t_{2g}(d_{xz/yz}, d_{xy})$. The three remaining $3d$ electrons occupy the spin-up V- d levels, forming an $e_g^2 t_{2g}^1$ configuration with a magnetic moment of approximately $3\mu_B$ according to the Hund's rule, which is close to the DFT calculation. The FM exchange coupling between neighboring V atoms within each layer is strongly enhanced by Hund's rule interaction due to empty t_{2g} orbitals [58]. The t_{2g} - t_{2g} superexchange of V atoms between adjacent layers via p orbitals of ligand is AFM due to the Goodenough-Kanamori-Anderson rule [58]. Furthermore, the Néel temperature for AFM- z V_2WS_4 is estimated as 490 K by Monte Carlo simulations [53].

AFM TI and topological invariant.— First we investigate the AFM- z ground state, which belongs to the type IV magnetic space group No. 114.282 in Belov-Neronova-Smirnova (BNS) notation [59]. The symmetry generators of this group include S_{4z} , $\Theta\tau_{1/2}$, C_{2z} and $C_{2x}\tau_{1/2}$. While the time-reversal symmetry Θ is broken, a combined symmetry $\mathcal{S} \equiv \Theta\tau_{1/2}$ is preserved, where $\tau_{1/2}$ is the half translation operator connecting neighboring W atomic layers, as marked in Fig. 1(a). This combined symmetry \mathcal{S} is antiunitary and satisfies $\mathcal{S}^2 = -e^{-2ik\cdot\tau_{1/2}}$. On

K	$\Gamma(000)$	$M(\pi\pi 0)$	$Z(00\pi)$	$A(\pi\pi\pi)$
$n_K^{1/2}, n_K^{-3/2}$	20, 20	20, 20	20, 20	19, 21

TABLE I. The number of occupied bands with S_{4z} eigenvalue $e^{-i\pi/4}$ and $e^{i3\pi/4}$ at four high symmetry points in BZ.

Brillouin-zone (BZ) plane where $\mathbf{k} \cdot \tau_{1/2} = 0$, $\mathcal{S}^2 = -1$. Therefore, similar to Θ in time-reversal-invariant (TRI) TI, \mathcal{S} enables a \mathcal{Z}_2 classification [19], where the \mathcal{Z}_2 topological invariant is well defined on the BZ plane with $\mathbf{k} \cdot \tau_{1/2} = 0$. The electronic structure without and with spin-orbital coupling (SOC) are shown in Fig. 2(a) and Fig. 2(b), respectively. One can see an anticrossing feature around Γ point from the band inversion between V $d_{xz,yz}$ orbitals and W d_{z^2} orbital, suggesting that V_2WS_4 might be topologically nontrivial. Since \mathcal{I} is broken but S_{4z} is preserved, the \mathcal{Z}_2 invariant is simply determined by the S_{4z} eigenvalues of the wavefunctions at S_{4z} -invariant momenta in the BZ [44], with the explicit form

$$\mathcal{Z}_2 = \sum_{K=\Gamma, M, Z, A} \frac{1}{2} \left(n_K^{\frac{1}{2}} - n_K^{-\frac{3}{2}} \right) \bmod 2, \quad (1)$$

where $n_K^{1/2}$ and $n_K^{-3/2}$ are the number of occupied states with S_{4z} eigenvalues $e^{-i\pi/4}$ and $e^{i3\pi/4}$, respectively. $K = \Gamma, M, Z, A$ are S_{4z} invariant in BZ. $n_K^{1/2}$ and $n_K^{-3/2}$ of high symmetry points are listed in Table I, so $\mathcal{Z}_2 = 1$. There are two additional symmetry indicators \mathcal{Z}_4 and δ_2 , which are used to characterize higher-order topology and Weyl semimetal [60, 61]. In the case of V_2WS_4 , both $\mathcal{Z}_4 = \delta_2 = 0$, as the Chern number for all k_z planes in the BZ is consistently zero. The monolayer is a FM QAH insulator [62], thus 3D AFM- z V_2WS_4 can be viewed as successive stacking of layered QAH with alternating Chern number $\mathcal{C} = \pm 1$, which are related by \mathcal{S} symmetry. We further employ the Willson loop method [63] to confirm the \mathcal{Z}_2 topological invariant in Fig. 2(h), concluding that AFM- z V_2WS_4 is indeed an AFM TI. Notably, we notice that a large energy gap of about 0.1 eV is obtained in Fig. 2(b).

One prominent feature of AFM TI is the existence of gapless surface states that depends on the crystallographic orientation of the surface plane, which is confirmed by the surface-state calculations. As shown in Fig. 2(f), the gapless surface states can be seen at Γ point forming a single Dirac cone in bulk gap on \mathcal{S} -preserving (110) surface. While the surface states are gapped on \mathcal{S} -broken (001) and (010) surfaces, as shown in Fig. 2(e) and Fig. 2(g), respectively.

Axion state and TME.— The $\mathcal{Z}_2 = 1$ topological invariant of AFM- z V_2WS_4 with a full band gap signifies the axion state with a quantized value $\theta = \pi \pmod{2\pi}$, where the electromagnetic response is described by the axion electrodynamics, $S_\theta = (\theta/2\pi)(\alpha/2\pi) \int d^3x dt \mathbf{E} \cdot \mathbf{B}$.

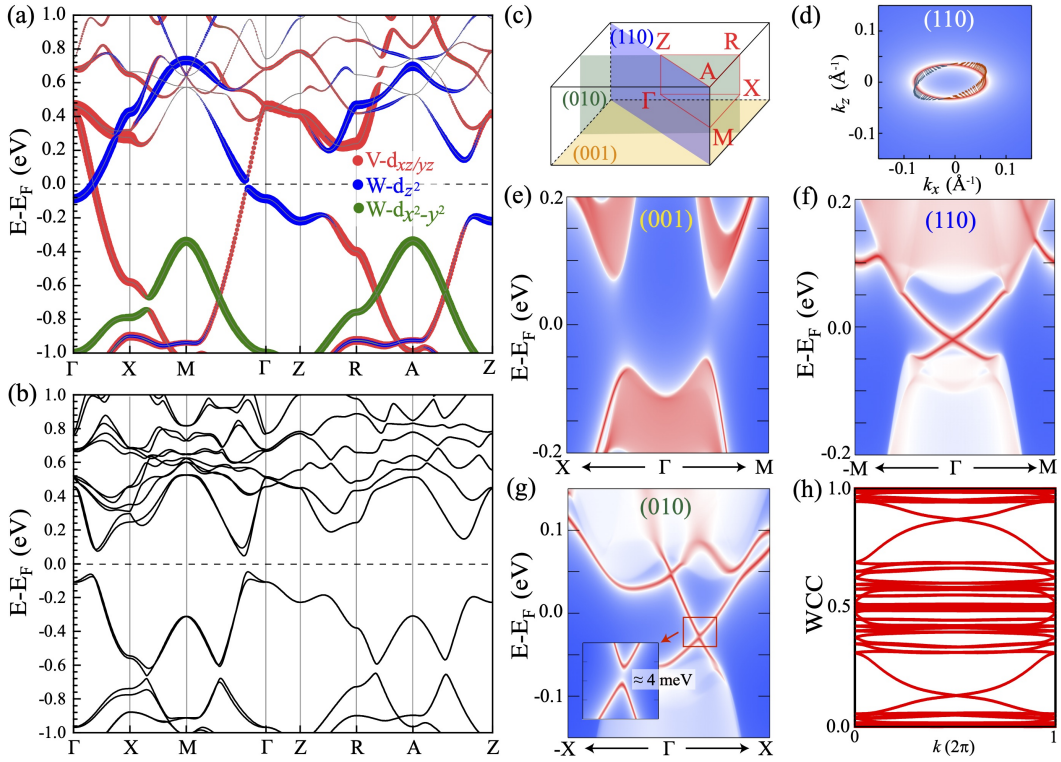


FIG. 2. Electronic structure and surfaces states of AFM- z V_2WS_4 . (a) The d -orbitals projected band structure without SOC, only those bands which are related to band inversion are highlighted. (b) Band structure with SOC. (c) Brillouin zone. (110), (001), and (001) surfaces are labeled as blue, orange, and green, respectively. (d) Fermi surface with spin texture on the (110) surface at Fermi level presents an ellipse shape. Blue and orange arrow of spin texture denote $s_y < 0$ and $s_y > 0$, respectively. (e)-(g) Surface states of the semi-infinite (001), (110) and (010) surfaces, respectively, which is gapless on the \mathcal{S} -preserving (110) surface, but gapped on the \mathcal{S} -broken (001) and (010) surfaces. (h) The Wannier charge centers (WCC) is calculated in the plane including TRI momenta (000) , $(\pi\pi 0)$, $(\pi 0\pi)$, and $(0\pi\pi)$ with $\mathbf{k} \cdot \tau_{1/2} = 0$, confirming $\mathcal{Z}_2 = 1$.

Here, \mathbf{E} and \mathbf{B} are the conventional electromagnetic fields inside the insulator, $\alpha = e^2/\hbar c$ is the fine-structure constant, e is electron charge, and θ is dimensionless pseudoscalar parameter [7]. This axion state gives rise to the TME, a phenomenon yet to be observed experimentally [3]. Interestingly, the gapped surface states from time-reversal symmetry breaking are naturally and intrinsically provided by even-layer V_2WS_4 films with A -type AFM structure, which make it an ideal platform for the long-sought quantized TME. Furthermore, to observe TME, all surface states must be gapped [23], which could be fulfilled by synthesizing realistic materials without any S -preserving surfaces. Compared to the previous proposals on TME in FM-TI heterostructure [7, 23, 24], the intrinsic magnetic TI material V_2WS_4 offer a more practical and promising avenue for exploring axion electrodynamics.

3D QAH state.— The AFM ground state of V_2WS_4 could be tuned to a FM configuration by applying an external magnetic field, leading to distinct topological phases. Here we study FM- z state, which belongs to magnetic space group No. 121.331 in BNS notation with symmetry generators S_{4z} , C_{2z} and ΘC_{2y} . For simplicity,

we adopted the conventional unit cell here as in AFM- z state. Then 3D FM- z V_2WS_4 can be interpreted as layer stacking of FM QAH insulator with the same Chern number $\mathcal{C} = -1$, leading to 3D QAH state or Weyl semimetal [12, 64]. The electronic structures without and with SOC are calculated in Fig. 3(a) and Fig. 3(b), respectively. There is spin polarized band inversion near the Fermi energy between spin up d_{xz}, d_{yz} bands of V and spin down d_{z^2} band of W, which is further gapped by SOC. Interestingly, along Γ -Z line, the band inversion always remains and there is no level crossing. Meanwhile, the FM- z state remains insulating, with a gap of approximately 20 meV. The Willson loop calculations shown in Fig. 3(c) reveal the Chern number $\mathcal{C} = -2$ at both $k_z = 0$ and $k_z = \pi$ planes, confirming that the system is a 3D QAH state. Moreover, our surface state calculations demonstrated the existence of chiral surface state on the (010) termination, which is the fingerprint of 3D QAH state. As shown in Fig. 3(d), two chiral edge states disperse within the bulk gap at $k_z = 0$ plane. Such chiral edge states extend over the entire surface BZ from $k_z = -\pi$ to $k_z = \pi$ plane without any Weyl points [Fig. 3(e)]. Thin films of 3D QAH insulator lead to the

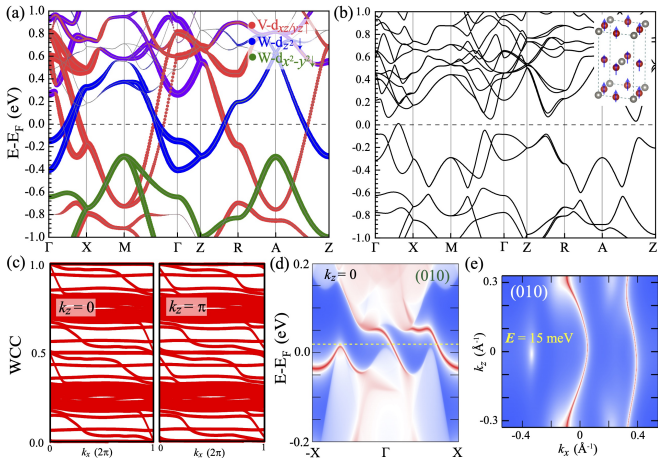


FIG. 3. Electronic structure and surfaces states of FM- z V_2WS_4 . (a) The d -orbital projected band structure without SOC. (b) Band structure with SOC. Here the conventional unit cell with FM- z state is chosen. (c) The evolution of WCC along the k_x direction in the $k_z = 0$ and $k_z = \pi$ plane. (d) Two chiral surface states on the semi-infinite (010) surface at $k_z = 0$. Consistent with WCC in (c), the Chern number is $\mathcal{C} = -2$ from $k_z = 0$ to $k_z = \pi$. (e) Fermi surface on the (010) termination at the isoenergy 15 meV above Fermi level. The chiral surface states extend over the entire surface BZ from $k_z = -\pi$ to $k_z = \pi$, indicating the 3D QAH state.

QAH effect in two dimensions (2D), the Chern number of which is equal to the layer number as will be discussed later. The high Chern number QAH effect with multiple dissipationless edge channels could lead to novel design of low energy cost electronic devices.

Tight-binding model and multilayer.— The layered van der Waals materials are featured by tunable quantum size effects. Here the band inversion in 3D suggests nontrivial topology may also exist in 2D multilayers. For AFM V_2WS_4 films, even and odd layers have distinct symmetry and topological properties. Even layers have S_{4z} and $C_{2x}\tau'_{1/2}$ symmetries, where $\tau'_{1/2} \equiv (a, a, 0)/2$, and all of the bands have Chern number $\mathcal{C} = 0$ because of the Hall conductance σ_{xy} is odd under $C_{2x}\tau'_{1/2}$. Differently, odd layers have S_{4z} and $C_{2x}\Theta$ symmetries, $\mathcal{C} \neq 0$ is allowed for σ_{xy} is invariant under $C_{2x}\Theta$. We construct a tight-binding model to recover the essential topological physics for AFM ground state, and investigate the crossover between bulk and multilayers.

From DFT calculations in Fig. 2, we construct the minimal tight-binding model including d_{xz}, d_{yz} of V and $d_{z^2}, d_{x^2-y^2}$ of W, where the band gap is mainly provided by the intralayer SOC effect with the opposite spin and interlayer orbital hopping with the same spin. The Hamiltonian is written as $\mathcal{H} = \begin{pmatrix} \mathcal{H}_1 & \mathcal{T} \\ \mathcal{T}^\dagger & \mathcal{H}_2 \end{pmatrix}$, where $\mathcal{H}_{1,2}$ are the intralayer Hamiltonian for two layers in the unit cell, \mathcal{T} is the interlayer hopping. For the intralayer, there are two V atoms, and d_{xz}, d_{yz} orbitals of each V are non-

degenerate. However, d_{xz} of one V and d_{yz} of the other V are degenerate, which are related to each other by S_{4z} . Therefore, for the low-energy physics of intralayer, for instance \mathcal{H}_1 , we only need to consider $d_{1,xz}^\uparrow, d_{1,yz}^\uparrow$ from two V, respectively and $d_{1,z^2}^\downarrow, d_{1,x^2-y^2}^\downarrow$ of W, namely a four orbitals model. \mathcal{H}_1 is obtained by considering the nearest-neighbor and next-nearest-neighbor hopping with SOC included. Then \mathcal{H}_2 of other layer is related to \mathcal{H}_1 by \mathcal{S} symmetry, where the spins are flipped with the basis of $d_2 \equiv (d_{2,xz}^\downarrow, d_{2,yz}^\downarrow, d_{2,z^2}^\uparrow, d_{2,x^2-y^2}^\uparrow)^T$. The interlayer hopping \mathcal{T} includes the orbital overlapping with the same spin, with the strength of about 50 meV which is smaller than the intralayer SOC. The explicit forms and fitted parameters are listed in Supplemental Material, where similar electronic structure and surface states of our model are obtained as DFT calculations [53].

By utilizing the tight-binding model, we can study the dimensional crossover from bulk to multilayer. As shown in Fig. 4, in AFM- z ground state, the band gap of multilayer shows oscillatory decay behavior and gradually converges to bulk value when the film exceed twenty layers, while the Chern number exhibit pronounced even-odd oscillations. The Chern number of band in a S_{4z} invariant system is $i^{\mathcal{C}} = \prod_{j \in \text{occupied}} (-1)^F \xi_j(\Gamma) \xi_j(M) \xi_j(X)$, with $F = 1$ for spinful case here, $\xi_j(k)$ is the S_{4z} eigenvalue at Γ and M points of the j -th band, $\xi_j(X)$ is the C_{2z} eigenvalue at X point on the j -th band [62]. Explicitly, odd layers have $\mathcal{C} = -1$, while even layers have $\mathcal{C} = 0$. Our DFT calculations up to seven layers are consistent with effective model [53]. These results suggest that multilayer V_2WS_4 can be viewed as layered stacking of alternating $\mathcal{C} = \pm 1$ QAH insulators for AFM- z state, or stacking of same $\mathcal{C} = -1$ QAH insulators for FM- z state, as illustrated in Fig. 4(a). The interlayer coupling is weaker than band inversion and SOC, thus the Chern number of multilayer is simply the summation of Chern number from each layer, namely

$$\mathcal{C}_{\text{multilayer}} = \sum_j \mathcal{C}_j. \quad (2)$$

Here $\mathcal{C}_j = \pm 1$ for each layer is only determined by the direction of magnetic moment, and does not affected by interlayer coupling.

It is insightful to compare V_2WS_4 with MnBi_2Te_4 , as both materials are layered van der Waals intrinsic magnetic TI with similar topological properties. In their AFM- z ground state, both are classified as AFM TIs and axion insulators in 3D, displaying an oscillation between zero and odd Chern numbers in AFM multilayers. However, their phases diverge significantly in the FM- z state. While V_2WS_4 is a 3D QAH state, MnBi_2Te_4 tends to be a Weyl semimetal or a trivial FM insulator [36, 37]. The primary distinctions arise from differences in interlayer coupling and band inversion. First, the low-energy physics in V_2WS_4 is from the d -orbitals

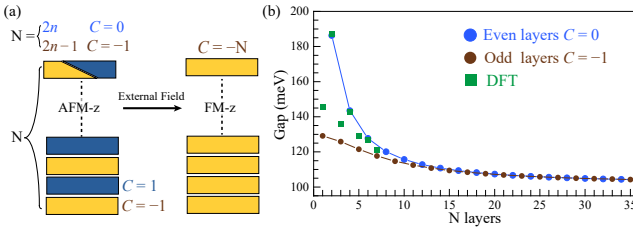


FIG. 4. (a) Schematic diagram shows layered stacking of QAH insulators with alternating Chern number $C = \pm 1$. In AFM- z state, it gives $C = -1$ QAH insulator in odd layers and $C = 0$ axion insulator in even layers. In FM- z state viewed as stacking of same Chern number $C = -1$ QAH insulators, N layers is a $C = -N$ high Chern number QAH insulator. (b) The evolution of band gap as a function of layer number in AFM- z state. Blue (brown) circle denotes even (odd) layers calculated from tight-binding model. Green box represents the gaps of one to seven layers by DFT calculations [53].

of V and W, which are located in the middle atomic layer. This contrasts with MnBi_2Te_4 , where the low-energy physics is dominated by the p_z orbitals of the outermost Bi/Te atomic layers. Consequently, the interlayer coupling is indirect and much weaker in V_2WS_4 compared to MnBi_2Te_4 (about 0.1 eV). Second, V_2WS_4 possesses much deeper band inversion. The band inversion point lie approximately at 35% along Γ - X line from Γ ($|\mathbf{k}| = 0.19 \text{ \AA}^{-1}$) as shown in Fig. 2(a), which is further opened by a strong SOC. The weak interlayer coupling could not change the band inversion along Γ - Z in V_2WS_4 . In contrast, the SOC induced band inversion is at Γ in MnBi_2Te_4 , then a relatively stronger interlayer coupling could modify the band inversion and lead to trivial insulators in few layers and Weyl semimetal in 3D. These distinctions highlight a key insight that such characteristics do not arise from fortuitousness in parameters, but rather from the universality inherent in V_2WS_4 family.

Discussion.— Other ternary transition metal chalcogenide, such as V_2WSe_4 , V_2MoX_4 and Ti_2WX_4 ($X = \text{S}$ or Se), which share the same orthorhombic crystal structure, are also promising candidates for hosting magnetic topological states similar to V_2WS_4 . In fact, most of them are found to be AFM TI in the ground state, as calculated in the Supplemental Material [53]. The synergy between intrinsic magnetism and topologically nontrivial bands, along with the variety of candidate materials, provides a rich platform for exploring emergent phenomena in magnetic topological states across different spatial dimensions. For instance, the magnetic fluctuations in these systems also give dynamic axion field.

The field of topological quantum matter in recent years developed explosively in materials science and condensed matter physics. One of main reasons is the precise theoretical predictions and experimental discovery of intrinsic topological materials. Tracing back the research history in magnetic topological physics, most of the previ-

ous experimental works are based on magnetically doped TIs and heterostructures [14–18, 25–28], which are quite complex and challenge to study [65, 66]. The research progress have been greatly prompted by discovering intrinsic magnetic TI material MnBi_2Te_4 [35, 40]. However, the co-antisite defects in Mn and Bi layers drastically suppress the exchange gap by several order of magnitude [67–69], which fundamentally deteriorates magnetic topological states. Meanwhile, few layers MnBi_2Te_4 with topologically nontrivial bands are too thick to tune efficiently. Finally, layered MnBi_2Te_4 usually contain Bi_2Te_3 layers, which further complicates the electronic structure with undesired topology. The V_2WS_4 -family materials satisfy all these material characteristics of simple, magnetic and topological. For example, monolayer V_2WS_4 is QAH insulator, in contrast to trivial FM insulator of monolayer MnBi_2Te_4 . Therefore, the techniques developed for 2D materials with versatile tunability can be readily applied to V_2WS_4 family. We anticipate that van der Waals heterostructures integrating V_2WS_4 family with other magnetic or superconducting 2D materials will provide fertile ground for exploring exotic topological quantum phenomena.

In summary, our work uncovers a large class of intrinsic magnetic TI materials with extremely rich topological quantum states of exceptional characteristics in different spatial dimensions. The broad range of candidate materials suggests that the underlying physics is quite general. We anticipate this will further enrich the magnetic TI family and provide a new material platform for exotic topological phenomena.

This work is supported by the Natural Science Foundation of China through Grants No. 12350404 and No. 12174066, the Innovation Program for Quantum Science and Technology through Grant No. 2021ZD0302600, the Science and Technology Commission of Shanghai Municipality under Grants No. 23JC1400600, No. 24LZ1400100 and No. 2019SHZDZX01. Y.J. acknowledges the support from China Postdoctoral Science Foundation under Grants No. GZC20240302 and No. 2024M760488.

* wjingphys@fudan.edu.cn

- [1] M. Z. Hasan and C. L. Kane, *Colloquium: Topological insulators*, *Rev. Mod. Phys.* **82**, 3045 (2010).
- [2] X.-L. Qi and S.-C. Zhang, *Topological insulators and superconductors*, *Rev. Mod. Phys.* **83**, 1057 (2011).
- [3] Y. Tokura, K. Yasuda, and A. Tsukazaki, *Magnetic topological insulators*, *Nature Rev. Phys.* **1**, 126 (2019).
- [4] J. Wang and S.-C. Zhang, *Topological states of condensed matter*, *Nature Mat.* **16**, 1062 (2017).
- [5] B. A. Bernevig, C. Felser, and H. Beidenkopf, *Progress and prospects in magnetic topological materials*, *Nature* **603**, 41 (2022).
- [6] C.-Z. Chang, C.-X. Liu, and A. H. MacDonald, *Collo-*

quium: Quantum anomalous hall effect, *Rev. Mod. Phys.* **95**, 011002 (2023).

[7] X.-L. Qi, T. L. Hughes, and S.-C. Zhang, Topological field theory of time-reversal invariant insulators, *Phys. Rev. B* **78**, 195424 (2008).

[8] A. M. Essin, J. E. Moore, and D. Vanderbilt, Magnetoelectric polarizability and axion electrodynamics in crystalline insulators, *Phys. Rev. Lett.* **102**, 146805 (2009).

[9] X.-L. Qi, R. Li, J. Zang, and S.-C. Zhang, Seeing the magnetic monopole through the mirror of topological surface states, *Science* **323**, 1184 (2009).

[10] Y. L. Chen, J.-H. Chu, J. G. Analytis, Z. K. Liu, K. Igarashi, H.-H. Kuo, X. L. Qi, S. K. Mo, R. G. Moore, D. H. Lu, M. Hashimoto, T. Sasagawa, S. C. Zhang, I. R. Fisher, Z. Hussain, and Z. X. Shen, Massive dirac fermion on the surface of a magnetically doped topological insulator, *Science* **329**, 659 (2010).

[11] R. Li, J. Wang, X. L. Qi, and S. C. Zhang, Dynamical axion field in topological magnetic insulators, *Nature Phys.* **6**, 284 (2010).

[12] J. Wang, B. Lian, and S.-C. Zhang, Dynamical axion field in a magnetic topological insulator superlattice, *Phys. Rev. B* **93**, 045115 (2016).

[13] R. Yu, W. Zhang, H.-J. Zhang, S.-C. Zhang, X. Dai, and Z. Fang, Quantized Anomalous Hall Effect in Magnetic Topological Insulators, *Science* **329**, 61 (2010).

[14] C.-Z. Chang, J. Zhang, X. Feng, J. Shen, Z. Zhang, M. Guo, K. Li, Y. Ou, P. Wei, L.-L. Wang, Z.-Q. Ji, Y. Feng, S. Ji, X. Chen, J. Jia, X. Dai, Z. Fang, S.-C. Zhang, K. He, Y. Wang, L. Lu, X.-C. Ma, and Q.-K. Xue, Experimental Observation of the Quantum Anomalous Hall Effect in a Magnetic Topological Insulator, *Science* **340**, 167 (2013).

[15] J. G. Checkelsky, R. Yoshimi, A. Tsukazaki, K. S. Takahashi, Y. Kozuka, J. Falson, M. Kawasaki, and Y. Tokura, Trajectory of the anomalous hall effect towards the quantized state in a ferromagnetic topological insulator, *Nature Phys.* **10**, 731 (2014).

[16] X. Kou, S.-T. Guo, Y. Fan, L. Pan, M. Lang, Y. Jiang, Q. Shao, T. Nie, K. Murata, J. Tang, Y. Wang, L. He, T.-K. Lee, W.-L. Lee, and K. L. Wang, Scale-invariant quantum anomalous hall effect in magnetic topological insulators beyond the two-dimensional limit, *Phys. Rev. Lett.* **113**, 137201 (2014).

[17] A. J. Bestwick, E. J. Fox, X. Kou, L. Pan, K. L. Wang, and D. Goldhaber-Gordon, Precise quantization of the anomalous hall effect near zero magnetic field, *Phys. Rev. Lett.* **114**, 187201 (2015).

[18] C.-Z. Chang, W. Zhao, D. Y. Kim, H. Zhang, B. A. As-saf, D. Heiman, S.-C. Zhang, C. Liu, M. H. W. Chan, and J. S. Moodera, High-precision realization of robust quantum anomalous hall state in a hard ferromagnetic topological insulator, *Nature Mater.* **14**, 473 (2015).

[19] R. S. K. Mong, A. M. Essin, and J. E. Moore, Antiferromagnetic topological insulators, *Phys. Rev. B* **81**, 245209 (2010).

[20] X. Wan, A. M. Turner, A. Vishwanath, and S. Y. Savrasov, Topological semimetal and fermi-arc surface states in the electronic structure of pyrochlore iridates, *Phys. Rev. B* **83**, 205101 (2011).

[21] G. Xu, H. Weng, Z. Wang, X. Dai, and Z. Fang, Chern Semimetal and the Quantized Anomalous Hall Effect in HgCr_2Se_4 , *Phys. Rev. Lett.* **107**, 186806 (2011).

[22] K. Nomura and N. Nagaosa, Surface-quantized anomalous hall current and the magnetoelectric effect in magnetically disordered topological insulators, *Phys. Rev. Lett.* **106**, 166802 (2011).

[23] J. Wang, B. Lian, X.-L. Qi, and S.-C. Zhang, Quantized topological magnetoelectric effect of the zero-plateau quantum anomalous Hall state, *Phys. Rev. B* **92**, 081107 (2015).

[24] T. Morimoto, A. Furusaki, and N. Nagaosa, Topological magnetoelectric effects in thin films of topological insulators, *Phys. Rev. B* **92**, 085113 (2015).

[25] M. Mogi, M. Kawamura, R. Yoshimi, A. Tsukazaki, Y. Kozuka, N. Shirakawa, K. S. Takahashi, M. Kawasaki, and Y. Tokura, A magnetic heterostructure of topological insulators as a candidate for an axion insulator, *Nature Mater.* **16**, 516 (2017).

[26] M. Mogi, M. Kawamura, A. Tsukazaki, R. Yoshimi, K. S. Takahashi, M. Kawasaki, and Y. Tokura, Tailoring tricolor structure of magnetic topological insulator for robust axion insulator, *Sci. Adv.* **3**, eaao1669 (2017).

[27] S. Grauer, K. M. Fijalkowski, S. Schreyeck, M. Wimmerlein, K. Brunner, R. Thomale, C. Gould, and L. W. Molenkamp, Scaling of the quantum anomalous hall effect as an indicator of axion electrodynamics, *Phys. Rev. Lett.* **118**, 246801 (2017).

[28] D. Xiao, J. Jiang, J.-H. Shin, W. Wang, F. Wang, Y.-F. Zhao, C. Liu, W. Wu, M. H. W. Chan, N. Samarth, and C.-Z. Chang, Realization of the Axion Insulator State in Quantum Anomalous Hall Sandwich Heterostructures, *Phys. Rev. Lett.* **120**, 056801 (2018).

[29] L. Fu and C. L. Kane, Superconducting proximity effect and majorana fermions at the surface of a topological insulator, *Phys. Rev. Lett.* **100**, 096407 (2008).

[30] L. Fu and C. L. Kane, Probing neutral majorana fermion edge modes with charge transport, *Phys. Rev. Lett.* **102**, 216403 (2009).

[31] X.-L. Qi, T. L. Hughes, and S.-C. Zhang, Chiral topological superconductor from the quantum hall state, *Phys. Rev. B* **82**, 184516 (2010).

[32] J. Wang, Q. Zhou, B. Lian, and S.-C. Zhang, Chiral topological superconductor and half-integer conductance plateau from quantum anomalous hall plateau transition, *Phys. Rev. B* **92**, 064520 (2015).

[33] B. Lian, X.-Q. Sun, A. Vaezi, X.-L. Qi, and S.-C. Zhang, Topological quantum computation based on chiral majorana fermions, *Proc. Natl. Acad. Sci. USA* **115**, 10938 (2018).

[34] J. Wang and B. Lian, Multiple chiral majorana fermion modes and quantum transport, *Phys. Rev. Lett.* **121**, 256801 (2018).

[35] Y. Deng, Y. Yu, M. Z. Shi, Z. Guo, Z. Xu, J. Wang, X. H. Chen, and Y. Zhang, Quantum anomalous hall effect in intrinsic magnetic topological insulator mnb_2te_4 , *Science* **367**, 895 (2020).

[36] D. Zhang, M. Shi, T. Zhu, D. Xing, H. Zhang, and J. Wang, Topological axion states in the magnetic insulator mnb_2te_4 with the quantized magnetoelectric effect, *Phys. Rev. Lett.* **122**, 206401 (2019).

[37] J. Li, Y. Li, S. Du, Z. Wang, B.-L. Gu, S.-C. Zhang, K. He, W. Duan, and Y. Xu, Intrinsic magnetic topological insulators in van der waals layered mnb_2te_4 -family materials, *Sci. Adv.* **5**, eaaw5685 (2019).

[38] M. M. Otrokov, I. I. Klimovskikh, H. Bentmann, A. Zeugner, Z. S. Aliev, S. Gass, A. U. B. Wolter, A. r. V. Koroleva, D. Estyunin, A. M. Shikin, M. Blanco-Rey,

M. Hoffmann, A. r. Y. Vyazovskaya, S. V. Eremeev, Y. M. Koroteev, I. R. Amiraslanov, M. B. Babanly, N. T. Mamedov, N. A. Abdullayev, V. N. Zverev, B. Büchner, E. F. Schwier, S. Kumar, A. Kimura, L. Petaccia, G. Di Santo, R. C. Vidal, S. Schatz, K. Kißner, C.-H. Min, S. K. Moser, T. R. F. Peixoto, F. Reinert, A. Ernst, P. M. Echenique, A. Isaeva, and E. V. Chulkov, Prediction and observation of an antiferromagnetic topological insulator, *Nature* **576**, 416 (2019).

[39] Y. Gong, J. Guo, J. Li, K. Zhu, M. Liao, X. Liu, Q. Zhang, L. Gu, L. Tang, X. Feng, D. Zhang, W. Li, C. Song, L. Wang, P. Yu, X. Chen, Y. Wang, H. Yao, W. Duan, Y. Xu, S.-C. Zhang, X. Ma, Q.-K. Xue, and K. He, Experimental realization of an intrinsic magnetic topological insulator, *Chin. Phys. Lett.* **36**, 076801 (2019).

[40] C. Liu, Y. Wang, H. Li, Y. Wu, Y. Li, J. Li, K. He, Y. Xu, J. Zhang, and Y. Wang, Robust axion insulator and chern insulator phases in a two-dimensional antiferromagnetic topological insulator, *Nature Mater.* **19**, 522 (2020).

[41] H. Deng, Z. Chen, A. Wołos, M. Konczykowski, K. Sobczak, J. Sitnicka, I. V. Fedorchenco, J. Borysiuk, T. Heider, Łukasz Pluciński, K. Park, A. B. Georgescu, J. Cano, and L. Krusin-Elbaum, High-temperature quantum anomalous hall regime in a $\text{mnb}_{2}\text{te}_4/\text{bi}_2\text{te}_3$ superlattice, *Nature Phys.* **17**, 36 (2021).

[42] B. Bradlyn, L. Elcoro, J. Cano, M. Vergniory, Z. Wang, C. Felser, M. Aroyo, and B. A. Bernevig, Topological quantum chemistry, *Nature* **547**, 298 (2017).

[43] J. Kruthoff, J. de Boer, J. van Wezel, C. L. Kane, and R.-J. Slager, Topological classification of crystalline insulators through band structure combinatorics, *Phys. Rev. X* **7**, 041069 (2017).

[44] L. Elcoro, B. J. Wieder, Z. Song, Y. Xu, B. Bradlyn, and B. A. Bernevig, Magnetic topological quantum chemistry, *Nature Commun.* **12**, 5965 (2021).

[45] H. C. Po, A. Vishwanath, and H. Watanabe, Symmetry-based indicators of band topology in the 230 space groups, *Nature Commun.* **8**, 50 (2017).

[46] H. Watanabe, H. C. Po, and A. Vishwanath, Structure and topology of band structures in the 1651 magnetic space groups, *Sci. Adv.* **4**, eaat8685 (2018).

[47] H. C. Po, Symmetry indicators of band topology, *J. Phys.: Condens. Matter* **32**, 263001 (2020).

[48] Y. Xu, L. Elcoro, Z.-D. Song, B. J. Wieder, M. G. Vergniory, N. Regnault, Y. Chen, C. Felser, and B. A. Bernevig, High-throughput calculations of magnetic topological materials, *Nature* **586**, 702 (2020).

[49] H. Xu, Y. Jiang, H. Wang, and J. Wang, Discovering two-dimensional magnetic topological insulators by machine learning, *Phys. Rev. B* **109**, 035122 (2024).

[50] Y.-J. Hao, P. Liu, Y. Feng, X.-M. Ma, E. F. Schwier, M. Arita, S. Kumar, C. Hu, R. Lu, M. Zeng, Y. Wang, Z. Hao, H.-Y. Sun, K. Zhang, J. Mei, N. Ni, L. Wu, K. Shimada, C. Chen, Q. Liu, and C. Liu, Gapless surface dirac cone in antiferromagnetic topological insulator $\text{mnb}_{2}\text{te}_4$, *Phys. Rev. X* **9**, 041038 (2019).

[51] H. Li, S.-Y. Gao, S.-F. Duan, Y.-F. Xu, K.-J. Zhu, S.-J. Tian, J.-C. Gao, W.-H. Fan, Z.-C. Rao, J.-R. Huang, J.-J. Li, D.-Y. Yan, Z.-T. Liu, W.-L. Liu, Y.-B. Huang, Y.-L. Li, Y. Liu, G.-B. Zhang, P. Zhang, T. Kondo, S. Shin, H.-C. Lei, Y.-G. Shi, W.-T. Zhang, H.-M. Weng, T. Qian, and H. Ding, Dirac surface states in intrinsic magnetic topological insulators $\text{eu}_{\text{n}}\text{s}_{\text{2}}\text{as}_{\text{2}}$ and $\text{mnb}_{2\text{n}}\text{te}_{3\text{n}+1}$, *Phys. Rev. X* **9**, 041039 (2019).

[52] Y. J. Chen, L. X. Xu, J. H. Li, Y. W. Li, H. Y. Wang, C. F. Zhang, H. Li, Y. Wu, A. J. Liang, C. Chen, S. W. Jung, C. Cacho, Y. H. Mao, S. Liu, M. X. Wang, Y. F. Guo, Y. Xu, Z. K. Liu, L. X. Yang, and Y. L. Chen, Topological electronic structure and its temperature evolution in antiferromagnetic topological insulator $\text{mnb}_{2}\text{te}_4$, *Phys. Rev. X* **9**, 041040 (2019).

[53] See Supplemental Material for technical details, which includes Refs. [70–82].

[54] C. J. Crossland, P. J. Hickey, and J. S. O. Evans, The synthesis and characterisation of cu_2mx_4 ($\text{m} = \text{w}$ or mo ; $\text{x} = \text{s}$, se or s/se) materials prepared by a solvothermal method, *J. Mater. Chem.* **15**, 3452 (2005).

[55] X. Hu, W. Shao, X. Hang, X. Zhang, W. Zhu, and Y. Xie, Superior electrical conductivity in hydrogenated layered ternary chalcogenide nanosheets for flexible all-solid-state supercapacitors, *Angew. Chem. Int. Ed.* **55**, 5733 (2016).

[56] F. Zhan, Q. Wang, Y. Li, X. Bo, Q. Wang, F. Gao, and C. Zhao, Low-temperature synthesis of cuboid silver tetrathiotungstate (ag_2ws_4) as electrocatalyst for hydrogen evolution reaction, *Inorg. Chem.* **57**, 5791 (2018).

[57] Y. Lin, S. Chen, K. Zhang, and L. Song, Recent advance of ternary layered cu_2mx_4 ($\text{m} = \text{mo}$, w ; $\text{x} = \text{s}$, se) nanomaterials for photocatalysis, *Solar RRL* **3**, 1800320 (2019).

[58] D. I. Khomskii, *Transition Metal Compounds* (Cambridge University Press, 2004).

[59] C. J. Bradley and A. P. Cracknell, *The Mathematical Theory of Symmetry in Solids* (Clarendon Press, Oxford, 1972).

[60] Z. Song, T. Zhang, Z. Fang, and C. Fang, Quantitative mappings between symmetry and topology in solids, *Nature Commun.* **9**, 3530 (2018).

[61] E. Khalaf, H. C. Po, A. Vishwanath, and H. Watanabe, Symmetry indicators and anomalous surface states of topological crystalline insulators, *Phys. Rev. X* **8**, 031070 (2018).

[62] Y. Jiang, H. Wang, K. Bao, Z. Liu, and J. Wang, Monolayer V_2MX_4 : A new family of quantum anomalous hall insulators, *Phys. Rev. Lett.* **132**, 106602 (2024).

[63] R. Yu, X. L. Qi, A. Bernevig, Z. Fang, and X. Dai, Equivalent expression of \mathbb{Z}_2 topological invariant for band insulators using the non-Abelian Berry connection, *Phys. Rev. B* **84**, 075119 (2011).

[64] A. A. Burkov and L. Balents, Weyl semimetal in a topological insulator multilayer, *Phys. Rev. Lett.* **107**, 127205 (2011).

[65] Y. X. Chong, X. Liu, R. Sharma, A. Kostin, G. Gu, K. Fujita, J. C. S. Davis, and P. O. Sprau, Severe dirac mass gap suppression in sb_2te_3 -based quantum anomalous hall materials, *Nano Lett.* **20**, 8001 (2020).

[66] E. O. Lachman, M. Mogi, J. Sarkar, A. Uri, K. Bagani, Y. Anahory, Y. Myasoedov, M. E. Huber, A. Tsukazaki, M. Kawasaki, Y. Tokura, and E. Zeldov, Observation of superparamagnetism in coexistence with quantum anomalous hall $c = \pm 1$ and $c = 0$ chern states, *npj Quantum Materials* **2**, 70 (2017).

[67] M. Garnica, M. M. Otrokov, P. C. Aguilar, I. I. Klimovskikh, D. Estyunin, Z. S. Aliev, I. R. Amiraslanov, N. A. Abdullayev, V. N. Zverev, M. B. Babanly, N. T. Mamedov, A. M. Shikin, A. Arnau, A. L. V. de Parga, E. V. Chulkov, and R. Miranda, Native point defects and their implications for the dirac point gap at

mnbi₂te4(0001), *npj Quantum Mater.* **7**, 7 (2022).

[68] H. Tan and B. Yan, Distinct magnetic gaps between anti-ferromagnetic and ferromagnetic orders driven by surface defects in the topological magnet mnbi₂te₄, *Phys. Rev. Lett.* **130**, 126702 (2023).

[69] X. Wu, C. Ruan, P. Tang, F. Kang, W. Duan, and J. Li, Irremovable mn-bi site mixing in mnbi₂te4, *Nano Lett.* **23**, 5048 (2023).

[70] G. Kresse and J. Furthmüller, Efficient iterative schemes for ab initio total-energy calculations using a plane-wave basis set, *Phys. Rev. B* **54**, 11169 (1996).

[71] P. E. Blöchl, Projector augmented-wave method, *Phys. Rev. B* **50**, 17953 (1994).

[72] J. P. Perdew, K. Burke, and M. Ernzerhof, Generalized gradient approximation made simple, *Phys. Rev. Lett.* **77**, 3865 (1996).

[73] S. Grimme, J. Antony, S. Ehrlich, and H. Krieg, A consistent and accurate ab initio parametrization of density functional dispersion correction (dft-d) for the 94 elements h-pu, *J. Chem. Phys.* **132**, 154104 (2010).

[74] S. Dudarev, G. Botton, S. Savrasov, C. Humphreys, and A. Sutton, Electron-energy-loss spectra and the structural stability of nickel oxide: An lsda+ u study, *Phys. Rev. B* **57**, 1505 (1998).

[75] A. A. Mostofi, J. R. Yates, Y.-S. Lee, I. Souza, D. Vanderbilt, and N. Marzari, wannier90: A tool for obtaining maximally-localised wannier functions, *Comput. Phys. Commun.* **178**, 685 (2008).

[76] Q. Wu, S. Zhang, H.-F. Song, M. Troyer, and A. A. Soluyanov, Wanniertools : An open-source software package for novel topological materials, *Comput. Phys. Commun.* **224**, 405 (2018).

[77] J. Gao, Q. Wu, C. Persson, and Z. Wang, Irvsp: To obtain irreducible representations of electronic states in the vasp, *Comput. Phys. Commun.* **261**, 107760 (2021).

[78] A. Togo and I. Tanaka, First principles phonon calculations in materials science, *Scr. Mater.* **108**, 1 (2015).

[79] X. He, N. Helbig, M. J. Verstraete, and E. Bousquet, Tb2j: A python package for computing magnetic interaction parameters, *Comput. Phys. Commun.* **264**, 107938 (2021).

[80] T. Ozaki, Variationally optimized atomic orbitals for large-scale electronic structures, *Phys. Rev. B* **67**, 155108 (2003).

[81] T. Ozaki and H. Kino, Numerical atomic basis orbitals from h to kr, *Phys. Rev. B* **69**, 195113 (2004).

[82] T. Ozaki and H. Kino, Efficient projector expansion for the ab initio lcao method, *Phys. Rev. B* **72**, 045121 (2005).